Tin negative electrodes using an FSA-based ionic liquid electrolyte: Improved performance of potassium secondary batteries

Takayuki Yamamoto,* Toshiyuki Nohira*

Institute of Advanced Energy, Kyoto University, Gokasho, Uji 611-0011, Japan

*Corresponding Authors:

*E-mail: yamamoto.takayuki.2w@kyoto-u.ac.jp, Tel: +81-774-38-3498, Fax: +81-774-38-3499 (T. Y.).

*E-mail: nohira.toshiyuki.8r@kyoto-u.ac.jp, Tel: +81-774-38-3500, Fax: +81-774-38-3499 (T. N.).

Abstract

In this study, submicron-sized tin particles were used as the negative electrode material for potassium secondary batteries. With a bis(fluorosulfonyl)amide-based ionic liquid electrolyte, K[FSA]–[C_3C_1pyrr][FSA], the tin negative electrodes showed improved capacity retention of over 170 mAh $(g\text{-}Sn)^{-1}$ after 100 cycles at room temperature.

Introduction

To make progress toward our ultimate goal of achieving and implementing sustainable energy systems without the use of conventional fossil fuels, closer collaboration between renewable energy resources and energy storage devices is essential to ensure a stable power supply. One possible solution is the wider distribution of large-scale batteries in households, buildings, industrial plants, etc. Although lithium secondary batteries currently installed in portable electric devices are promising candidates, the scarcity of lithium and cobalt resources and the flammability of organic-solvent-based electrolytes increase the likelihood of future price hike and the risk of fatal accidents. Thus, in recent decades, tremendous efforts have been devoted to the development of alternative batteries that use abundant resources and safer electrolytes.[1–5]

We are now focusing on potassium secondary batteries using ionic liquid (IL) electrolytes. Potassium resources are plentiful in the Earth's crust and seawater, resulting in their low cost and wider distribution of large-scale battery systems. Moreover, inexpensive aluminum current collectors can be used for the negative electrodes of potassium secondary batteries, whereas the more costly copper is needed for their lithium counterparts. Moreover, ILs are known to be safer electrolytes because of their negligible volatility and nonflammability; they are widely studied as electrolytes in batteries, fuel cells, capacitors, and other devices. Several groups, including ours, have reported the physicochemical properties of IL electrolytes for potassium secondary batteries.[6–9] One important advantage is the wider electrochemical window of potassium-based IL electrolytes compared with those of lithium- and sodium-based ones.[7,9] For example, the redox potentials of M^+/M (M = Li, Na, K) were compared in

the M[FSA]–[C_3C_1pyrr][FSA] IL (FSA = bis(fluorosulfonyl)amide, C_3C_1pyrr = *N*-methyl-*N*-propylpyrrolidinium).[7] The redox potential of K^+/K is more negative than that of Na^+/Na by 0.35 V and even that of Li^+/Li by 0.25 V, whereas the anodic decomposition potentials are almost equal within experimental error. Furthermore, the use of this potassium-based IL is beneficial in terms of stability against potassium metal. In some types of organic-solvent-based electrolytes, potassium metal does not work effectively as a counter electrode in a two electrode-type cell.[10] In the K[FSA]–[C_3C_1pyrr][FSA] IL, on the other hand, we recently evaluated the charge–discharge behavior of alloy-based negative electrodes with two-electrode coin cells using a potassium metal counter electrode and obtained reasonably high performance.[11] These results imply the superiority of this IL in long-term durability, especially in the negative potential region.

In this study, tin negative electrodes prepared from commercial submicron-sized tin particles are used with the IL electrolyte, and their fundamental electrochemical behavior is investigated via galvanostatic charge–discharge (GCD) tests, galvanostatic intermittent titration technique (GITT), X-ray diffraction (XRD), and field emission scanning electron microscopy (FE-SEM).

Experimental Section

The K[FSA]–[C_3C_1pyrr][FSA] IL (x(K[FSA]) = 0.20, where x(K[FSA]) = molar fraction of K[FSA]; $C(K^+)$ = ca. 1 mol dm^{-3}) was prepared by mixing K[FSA] and [C_3C_1pyrr][FSA]. The tin negative electrodes were composed of tin powder (paricle size: 100–200 nm) as the active material, acetylene carbon black (AB) powder as a conductive agent, and polyamide-imide (PAI) as a binder, with a weight ratio of

80/10/10. To prepare the electrodes (denoted as Sn/AB/PAI electrodes) the active material, conductive agent, and binder were mixed in *N*-methyl-2-pyrrolidone (NMP) and the resultant slurry was coated onto aluminum foil. The NMP was then removed at 353 K for 3 h in a vacuum, and the electrodes were punched out of the foil as circles with diameter 10 mm. The electrodes were dried at 363 K overnight in a vacuum of < 1 Pa. The tin loading masses were controlled within the range of 2.0–2.6 (mg-Sn) cm^{-2}.

Results and Discussion

Fig. 1 shows representative charge–discharge curves of the Sn/AB/PAI electrode in the K[FSA]–[C_3C_1pyrr][FSA] (*x*(K[FSA]) = 0.20) IL at a charge–discharge rate of 20 mA $(g\text{-Sn})^{-1}$. In the 1st charge (potassiation) process, several plateaus and slopes are observed in the voltage region below 1.5 V. The capacity from a small plateau at approximately 1.35 V and a slope region at around 1.0 V may correspond to the irreversible formation of a solid electrolyte interphase (SEI), because amide-based ILs give similar behavior with carbon-based negative electrodes.[12,13] According to previous reports of K–Sn alloy formation in organic-solvent-based electrolytes,[14–22] a slope region at around 0.5 V and a long plateau at 0.17 V include the potassiation reaction of tin. In contrast, the 1st discharge curve consists of multiple short plateaus, suggesting the existence of several K–Sn alloy phases. The charge and discharge capacities obtained in the 1st cycle are 328 and 167 mAh $(g\text{-Sn})^{-1}$, respectively. Table S1 summarizes the K–Sn alloy phases reported in papers on the phase diagram and on structure determination. The 1st discharge capacity lies between the theoretical capacities for K_2Sn_3 and KSn formation. Except for the 1st charge, the charge–discharge curves in the initial 5 cycles almost overlap with each other, indicating stable charge–

discharge cycling. This is also supported by morphological observation by FE-SEM, as shown in Fig. 2. On the surfaces of the Sn/AB/PAI electrodes, only minor morphological change was confirmed after 5 cycles. Additionally, rate capability was investigated as shown in Fig. S2. The tin electrode maintains a capacity of 117 mAh $(g\text{-}Sn)^{-1}$ at a rate of 100 mA $(g\text{-}Sn)^{-1}$.

The formation of K–Sn alloy phases was confirmed by X-ray diffraction on the fully charged state. Fig. 3 shows the diffraction pattern of the fully charged Sn/AB/PAI electrode prepared by the combination of galvanostatic charging and open-circuit potential relaxation. Several peaks at diffraction angles $2\theta \approx 14.5°$ (index: 112), 28.6° (321), and 29.7° (215) are ascribed to the KSn phase. However, the intensities of other diffraction peaks are very low, owing to the low crystallinity of the electrochemically formed K–Sn alloy. Similar behavior has been observed in the electrochemical formation of Na–Sn alloys.[23] In addition, β-Sn peaks are also present, either because the active material remained partially unreacted, or because the K–Sn alloys produced are decomposed into pure tin and potassium hydroxide by incomplete airtightness of the supposedly air-tight XRD cell. According to the phase diagram, the most potassium-rich phase is K_2Sn, whose crystal structure is unknown. However, in some reports on tin-based negative electrodes for potassium secondary batteries using organic-solvent-based electrolytes,[15,17,20,21] KSn is the richest phase in the electrochemical reaction. In the present study on the FSA-based IL electrolyte, the fully charged state of the Sn/AB/PAI electrode is reasonably considered to be KSn, based on the reversible capacities and the X-ray diffraction results.

Further investigation was conducted by the galvanostatic intermittent titration technique (GITT), as shown in Fig. S1. The GITT measurements after 1 charge–

discharge cycle indicate the existence of several slope and plateau regions during the charging process, as observed in the galvanostatic charge–discharge tests. The capacity at the end of the slope corresponds to the theoretical capacity of K_8Sn_{46} (K_4Sn_{23}). The subsequent long plateau at 0.35 V vs. K^+/K continues over the compositional range $0.2 < x < 0.7$ of K_xSn. Judging from the list of K–Sn alloy phases (Table S1), this plateau is attributed to the equilibrium between K_8Sn_{46} ($x = 0.17$) and K_2Sn_3 ($x = 0.67$). The final slope reaches almost 0 V vs. K^+/K at the composition where $x = 1.19$ (270 mAh $(g\text{-}Sn)^{-1}$), which slightly exceeds that of the K–Sn alloy phase (KSn; $x = 1$) observed by X-ray diffraction. This phenomenon may have two possible explanations: (1) irreversible decomposition of the electrolyte at lower potential, or (2) the existence of a solid-solution compositional region at around $x = 1$. In contrast, multiple plateaus are confirmed in the discharging process (Fig. S1c), which is consistent with the results of the charge–discharge test (See Fig. 1 and Fig. S1a).

Since dealloying of K–Sn alloys begins from the second plot at 0 V vs. K^+/K, we tentatively assume that this point corresponds to the most potassium-rich composition of the K–Sn alloy, *i.e.*, $x_{max} = 1.19$. The first sloping region between 0 and 0.5 V is typical behavior for solid solutions, implying the possibility (2) proposed above in the discussion of the charging GITT measurements. In the compositional range $x < 1$, the profile of the open circuit potentials is roughly divided into several parts, as described by the broken lines. Although this assignment almost agrees with the reported K–Sn alloy phases, further detailed examination is needed in the future. Finally, the proportion (x) of potassium in tin comes back to nearly zero, indicating that the fully discharged state is pure metallic tin.

The prolonged charge–discharge performance was evaluated for Sn/AB/PAI

electrodes at room temperature. According to the charge–discharge curves shown in Fig. 4a, the charging (potassiation) profiles are stable for 100 cycles, except for the 1st cycle. Concerning the discharge (depotassiation) process, the polarization of plateaus at around 1.0 V becomes slightly larger after the 10th cycle, whereas no significant change is confirmed in the middle plateau region at around 0.7 V. Such a different trend is possibly explained by the degree of volume contraction for each reaction step. When the discharge reactions are expressed with K–Sn alloy phases whose structures are known (Eqs. 1 and 2), the contraction ratios are calculated to be 0.50 (= 16.29/32.67) for region (A) at ca. 1.0 V and 0.72 (= 32.67/45.58) for region (B) at ca. 0.7 V, using the molar volumes of K–Sn alloys summarized in Table S1.

(Region (A) at ca. 1.0 V) $K_4Sn_9 \rightarrow 9\ Sn + 4\ K^+ + 4\ e^-$ (1)

(Region (B) at ca. 0.7 V) $9\ KSn \rightarrow K_4Sn_9 + 5\ K^+ + 5\ e^-$ (2)

Since the contraction ratio is lower for region (A), the degradation will progress faster for that reaction, leading to large polarization in the earlier cycles. Similar behavior was also confirmed in our previous studies on Na–Sn negative electrodes.[24] Fig. 4b shows cycling properties of the Sn/AB/PAI electrode for 100 cycles at room temperature. The discharge capacity at the 100th cycle is 173 mAh $(g\text{-}Sn)^{-1}$, corresponding to a capacity retention ratio of 93% with respect to the 1st cycle. The average coulombic efficiency (except for the 1st cycle) is 97.5% over 100 cycles. In addition, a charge–discharge test at elevated temperature was conducted to study the improvement in reversible capacities. As shown in Fig. S3, although the capacity increased to nearly 200 mAh $(g\text{-}Sn)^{-1}$ at 313 K, the production of phases more potassium-rich than KSn is unlikely. Thus, further studies are necessary to elucidate the K–Sn formation mechanism.

Table 1 summarizes the present and previous studies on tin negative electrodes for

potassium secondary batteries, in which organic-solvent-based electrolytes were utilized in all cases except ours. One important point to be mentioned is the operating voltage range. Most studies adopt upper cut-off voltages higher than 1.5 V;[14,16–19,21,22] however, such operation ranges wider than 1.5 V are not realistic conditions for practical batteries. In addition to the reported initial discharge capacities, the estimated initial capacities and n^{th} cycle capacities, based on a realistic upper cut-off voltage of 1.2 V, are given in the middle and right columns of the discharge capacity. Several previous studies achieved relatively high initial capacities of over 200 mAh g^{-1} even for a realistic voltage range, but a large deterioration in capacity was observed after prolonged cycling. In the present study, however, the highest capacity of 173 mAh g^{-1} was retained even after 100 cycles. Simple commercial tin powders with no carbon coating exhibit reasonably high capacities and decent cycling properties in the FSA-based IL electrolyte, because of the stability of the IL in negative potential regions. In other words, stable SEI film formation may give superior durability of tin negative electrodes, as with the case of negative electrodes for sodium secondary batteries.[5,13]

Conclusions

In conclusion, the charge–discharge behavior of tin negative electrodes has been evaluated using the K[FSA]–[C_3C_1pyrr][FSA] IL electrolyte. The Sn/AB/PAI electrodes showed high capacities of over 170 mAh $(g\text{-}Sn)^{-1}$, stable over 100 cycles at room temperature, owing to the electrochemical stability of the IL. The electrochemical alloying/dealloying mechanism was partly clarified by a combination of the galvanostatic intermittent titration technique and X-ray diffraction. To further enhance the performance of potassium secondary batteries, the mismatch between phase

diagrams and observed capacities needs to be resolved in future studies.

Acknowledgments

This study was partly supported by JSPS KAKENHI grant (JP18K14320) and the research grant of Izumi Science and Technology Foundation. We thank Nippon Shokubai Co., Ltd. for supplying K[FSA]. The polyamide-imide binder was provided by Profs. R. Hagiwara and K. Matsumoto in Kyoto University.

Conflicts of interest

The authors declare no competing financial interest.

References

1 N. Yabuuchi, K. Kubota, M. Dahbi and S. Komaba, *Chem. Rev.*, 2014, **114**, 11636−11682.

2 D. Larcher and J-M. Tarascon, *Nat. Chem.*, 2015, **7**, 19–29.

3 M. Watanabe, M. L. Thomas, S. Zhang, K. Ueno, T. Yasuda and K. Dokko, *Chem. Rev.*, 2017, **117**, 7190–7239.

4 A. Eftekhari, Z. Jian and X. Ji, *ACS Appl. Mater. Interfaces*, 2017, **9**, 4404–4419.

5 K. Matsumoto, J. Hwang, S. Kaushik, C-Y. Chen and R. Hagiwara, *Energy Environ. Sci.,* 2019, **12**, 3247–3287.

6 K. Beltrop, S. Beuker, A. Heckmann, M. Winter and T. Plack, *Energy Environ. Sci.*, 2017, **10**, 2090–2094.

7 T. Yamamoto, K. Matsumoto, R. Hagiwara, T. Nohira, *J. Phys. Chem. C*, 2017, **121**,

18450–18458.

8 T. Masese, K. Yoshii, Y. Yamaguchi, T. Okumura, Z-D. Huang, M. Kato, K. Kubota, J. Furutani, Y. Orikasa, H. Senoh, H. Sakaebe and M. Shikano, *Nat. Commun.*, 2018, **9**, 3823.

9 K. Yoshii, T. Masese, M. Kato, K. Kubota, H. Senoh and M. Shikano, *ChemElectroChem*, 2019, **6**, 3901–3910.

10 T. Hosaka, S. Muratsubaki, K. Kubota, H. Onuma and S. Komaba, *J. Phys. Chem. Lett.*, 2019, **10**, 3296–3300.

11 Y. Domi, H. Usui, E. Nakabayashi, T. Yamamoto, T. Nohira and H. Sakaguchi, *Electrochemistry*, 2019, **87**, 333–335.

12 A. Fukunaga, T. Nohira, R. Hagiwara, K. Numata, E. Itani, S. Sakai, K. Nitta and S. Inazawa, *J. Power Sources*, 2014, **246**, 387–391.

13 T. Yamamoto, T. Yamaguchi, T. Nohira, R. Hagiwara, A. Fukunaga, S. Sakai and K. Nitta, *Electrochemistry*, 2017, **85**, 391–396.

14 I. Sultana, T. Ramireddy, M. M. Rahman, Y. Chen and A. M. Glushenkov, *Chem. Commun.*, 2016, **52**, 9279–9282.

15 T. Ramireddy, R. Kali, M. K. Jangid, V. Srihari, H. K. Poswal and A. Mukhopadhyay, *J. Electrochem. Soc.*, 2017, **164**, A2360–A2367.

16 Q. Wang, X. Zhao, C. Ni, H. Tian, J. Li, Z. Zhang, S. X. Mao, J. Wang and Y. Xu, *J. Phys. Chem. C*, 2017, **121**, 12652–12657.

17 W. Zhang, J. Mao, S. Li, Z. Chen and Z. Guo, *J. Am. Chem. Soc.*, 2017, **139**, 3316–3319.

18 K. Huang, Z. Xing, L. Wang, X. Wu, W. Zhao, X. Qi, H. Wang and Z. Ju, *J. Mater. Chem. A*, 2018, **6**, 434–442.

19 M. Shimizu, R. Yatsuzuka, T. Koya, T. Yamakami and S. Arai, *ACS Appl. Energy Mater.*, 2018, **1**, 6865–6870.

20 V. Gabaudan, R. Berthelot, M. T. Sougrati, P-E. Lippens, L. Monconduit and L. Stievano, *J. Mater. Chem. A*, 2019, **7**, 15262–15270.

21 H. Wang, Z. Xing, Z. Hu, Y. Zhang, Y. Hu, Y. Sun, Z. Ju and Q. Zhuang, *Appl. Mater. Today*, 2019, **15**, 58–66.

22 Y. Yang, D. Li, J. Zhang, G. Suo, Q. Yu, L. Feng, X. Hou, X. Ye, L. Zhang and W. Wang, *Mater. Lett.*, 2019, **256**, 126613.

23 T. Yamamoto, T. Nohira, R. Hagiwara, A. Fukunaga, S. Sakai, K. Nitta and S. Inazawa, *J. Power Sources*, 2013, **237**, 98–103.

24 T. Yamamoto, T. Nohira, R. Hagiwara, A. Fukunaga, S. Sakai, K. Nitta, S. Inazawa, *J. Power Sources*, 2012, **217**, 479–484.

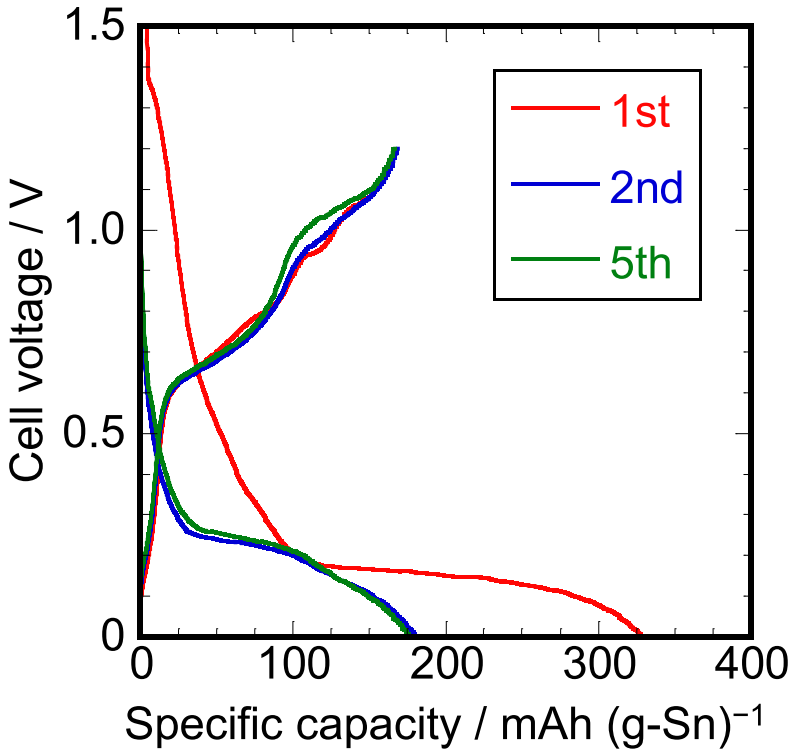

Fig. 1 Charge–discharge curves of the Sn/AB/PAI electrode in K[FSA]–[C_3C_1pyrr][FSA] IL electrolyte for 5 cycles at 298 K. Charge–discharge rate: 20 mA (g-Sn)$^{-1}$.

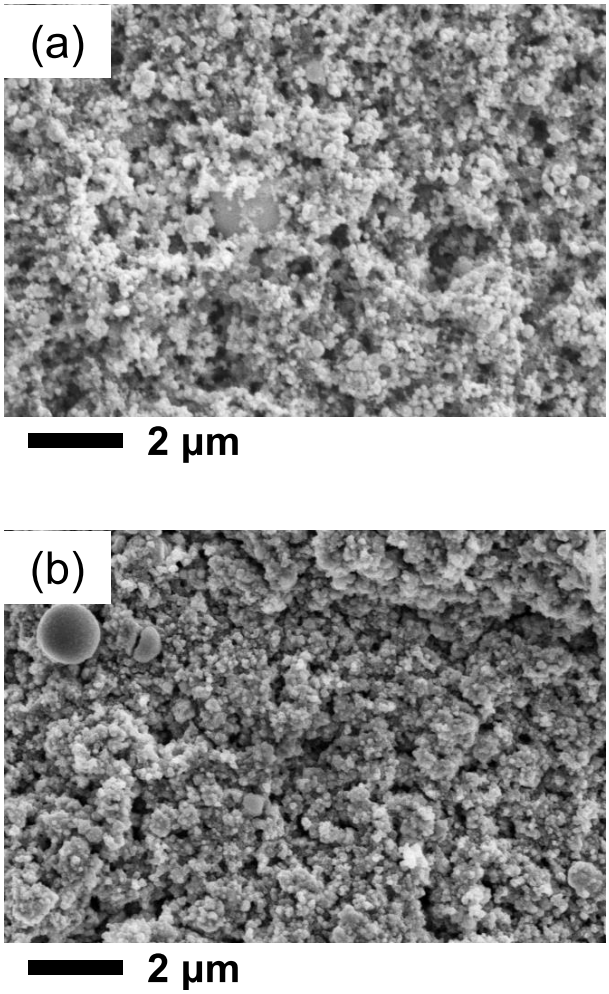

Fig. 2 Representative FE-SEM images of Sn/AB/PAI electrodes (a) before the test and (b) after 5 charge–discharge cycles.

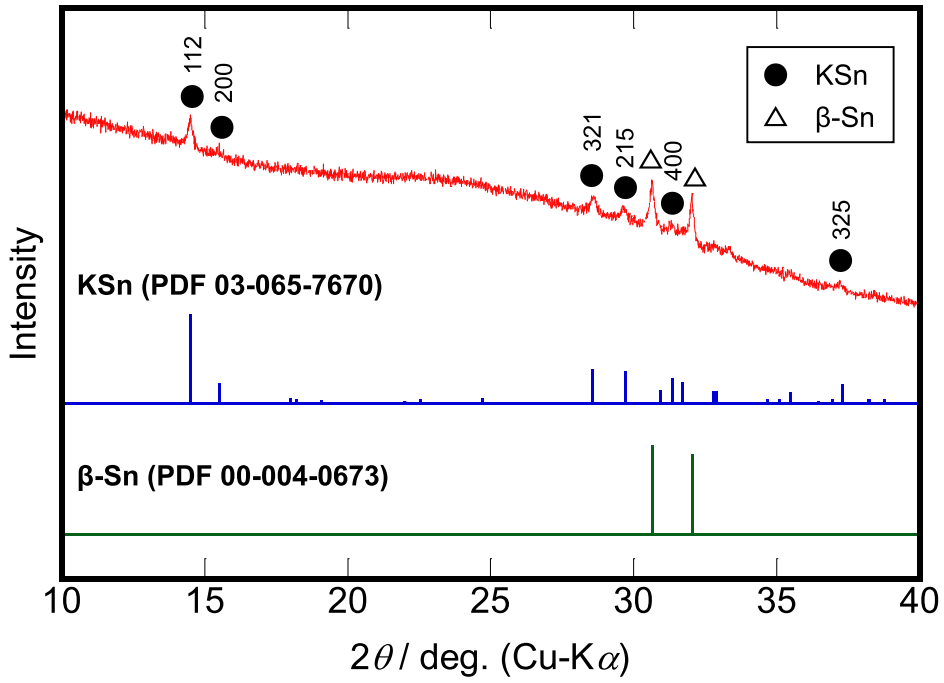

Fig. 3 X-ray diffraction pattern of the fully charged Sn/AB/PAI electrode.

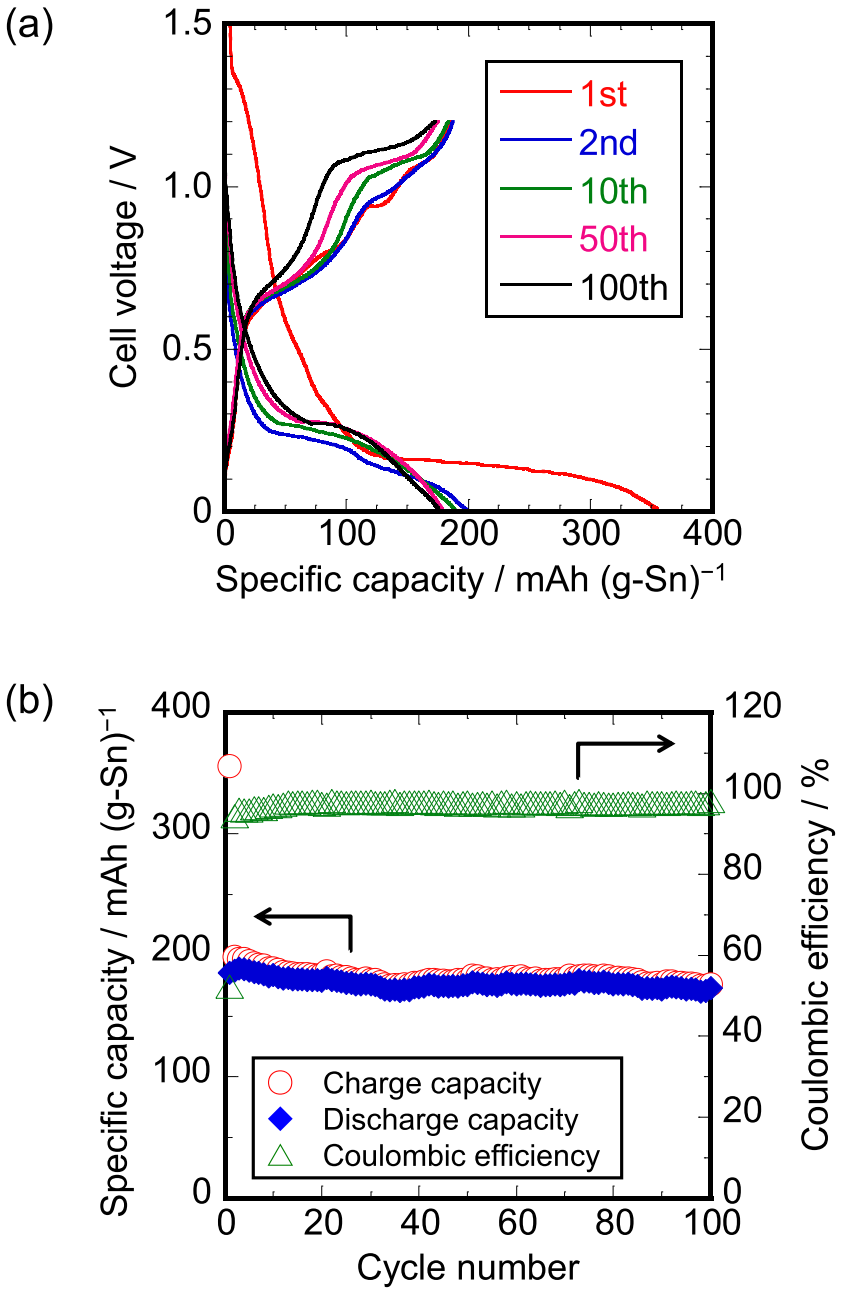

Fig. 4 (a) Charge–discharge curves, and (b) cycling properties of specific capacities and Coulombic efficiencies of the Sn/AB/PAI electrode in K[FSA]–[C_3C_1pyrr][FSA] IL electrolyte at 298 K. Charge–discharge rate: 20 mA (g-Sn)$^{-1}$.

Table 1 Comparison of present and previous studies on tin negative electrodes for potassium secondary batteries.

Type of tin electrode (particle size)	Electrolyte	Discharge capacity / mAh (g-active material)$^{-1}$			Charge–discharge rate / mA g^{-1}	Active material	Binder**	Ref.
		1st cycle (Cut-off voltage)	1st cycle (< 1.2 V)	n^{th} cycle (< 1.2 V)				
Sn powder (100–200 nm)	1 mol dm^{-3} K[FSA]–[C_3C_1pyrr][FSA]	186 (0.005–1.2 V)	186	173 (100th)	20	Sn	PAI	This study
Sn–C composite	0.75 mol dm^{-3} KPF_6 in EC–DEC	140 (0.01–2.0 V)	~100	~80 (15th)	25	Sn+C	CMC	14
200 nm thin Sn film	1 mol dm^{-3} KPF_6 in EC–DEC	~225 (0.01–1.2 V)	~225	85 (20th)	25	Sn	–	15
Sn powder (70–350 nm)	0.8 mol dm^{-3} KPF_6 in EC–DEC	197 (0.01–2 V)	~180	< 50 (10th)	20	Sn	SA	16
Sn/C composite	0.8 mol dm^{-3} KPF_6 in EC–DEC	~200 (0.01–2 V)	~150	< 50 (30th)	50	Sn	CMC	17
porous carbon/Sn composite	0.8 mol dm^{-3} $KClO_4$ in EC–DEC	385 (0.01–3 V)	~190	~140 (100th)	50	Sn+C	PVdF	18
Sn powder (70–500 nm)	0.5 mol dm^{-3} KPF_6 in EC–DEC	229 (0.005–2.0 V)	~210	< 50 (20th)	25	Sn	CMC–SBR	19
Sn powder	0.8 mol dm^{-3} KFSA in EC–DEC	~240 (0.0–1.1 V)	~240 (0.0–1.1 V)	~110 (50th)	23	Sn*	CMC	20
Sn@RGO	0.8 mol dm^{-3} KPF_6 in EC–DEC	~240 (0.001–3.0 V)	~140	~115 (50th)	100	Sn+C	CMC	21
Sn nanoparticles anchored on N doped porous carbon	1 mol dm^{-3} KPF_6 in EC–DEC	286 (0.01–2.6 V)	~125	~90 (100th)	50	Sn+C	PVdF	22

* The capacities were recalculated based on the composition of the tin electrode.
** PAI = polyamide-imide, CMC = carboxymethyl cellulose, SA = sodium alginate, PVdF = polyvinylidene difluoride, SBR = styrene butadiene rubber

Electronic Supplementary Information (ESI)

Tin negative electrodes using an FSA-based ionic liquid electrolyte: Improved performance of potassium secondary batteries

Takayuki Yamamoto,* and Toshiyuki Nohira *

Institute of Advanced Energy, Kyoto University, Gokasho, Uji 611-0011, Japan

*Corresponding Authors:

*E-mail: yamamoto.takayuki.2w@kyoto-u.ac.jp, Tel: +81-774-38-3498, Fax: +81-774-38-3499 (T. Y.).

*E-mail: nohira.toshiyuki.8r@kyoto-u.ac.jp, Tel: +81-774-38-3500, Fax: +81-774-38-3499 (T. N.).

Experimental Details

K[FSA] (purity > 99%; supplied from Nippon Shokubai Co., Ltd.) and [C_3C_1pyrr][FSA] (> 99.9%; Kanto Chemical Co., Inc.) were dried under vacuum at 333 K or above. Tin powder (Sigma-Aldrich, Inc.) and acetylene black (Strem Chemicals, Inc.) was used as received. The electrochemical measurements were conducted using 2032-type coin cells and electrochemical measurement apparatuses (HZ-Pro, Hokuto Denko Corp., or VSP, Bio-Logic Co.). In the coin cells, Sn/AB/PAI electrodes and potassium metal were used as working and counter electrodes, respectively. A two-ply glass-fiber filter paper (Whatman, GF/A, 260 mm) was used as a separator. The working electrodes and separator were vacuum-impregnated with the K[FSA]–[C_3C_1pyrr][FSA] electrolyte prior to the test.

Galvanostatic intermittent titration technique (GITT) was employed according to the following procedure:

1. Galvanostatic electrolysis was conducted at a current density of 10 mAh $(\text{g-Sn})^{-1}$ for 1 h (*i.e.*, 10 mAh $(\text{g-Sn})^{-1}$). If the cell voltage reaches −0.1 V (charging) and +1.5 V (discharging), move onto step 2 immediately.
2. The open circuit potential was monitored, and the potential after 3 hours was regarded as the equilibrium value.

3. Steps 1 and 2 were repeated 30 times in total.

To identify the existing phases of the charged Sn/AB/PAI electrode, X-ray diffraction (XRD) analysis was performed using an X-ray diffractometer (Ultima IV, Rigaku Co.; Cu-Kα radiation (λ = 0.15418 nm)) equipped with a 1D high-speed detector (D/teX Ultra, Rigaku Co.) with a nickel filter. The surface of the Sn/AB/PAI electrodes were observed with a field emission scanning electron microscope (FE-SEM; SU-6600, Hitachi). Before these analyses, the electrochemical cells were disassembled and the remaining electrolytes in Sn/AB/PAI electrodes were removed by soaking the samples in dehydrated and deoxidized tetrahydrofuran (water content < 10 ppm, oxygen content < 1 ppm; Wako Pure Chemical Industries, Ltd.). All the reagents were handled in the argon-filled glovebox. The samples were transferred to the X-ray diffractometer and a field emission scanning electron microscope without air exposure.

Table S1 Reported K–Sn alloy phases and the corresponding capacities, compositions, and molar volumes.

Phase	Capacity / mAh (g-Sn)$^{-1}$	Composition x (in K_xSn)	Molar volume / cm^3 (mol-Sn)$^{-1}$	Ref.
Sn	0	0	16.29	[a]
K_8Sn_{46}	39	0.17	22.79	[b]
K_6Sn_{25}*	54	0.24	25.61	[c]
K_4Sn_9*	100	0.44	32.67	[d]
KSn_2**	113	0.50	N.A.	[a]
K_2Sn_3**	151	0.67	N.A.	[a]
KSn	226	1.00	45.58	[e]
K_2Sn**	452	2.00	N.A.	[a]

* The phase is not shown in the K–Sn phase diagram [a].

** Crystal structure is unknown.

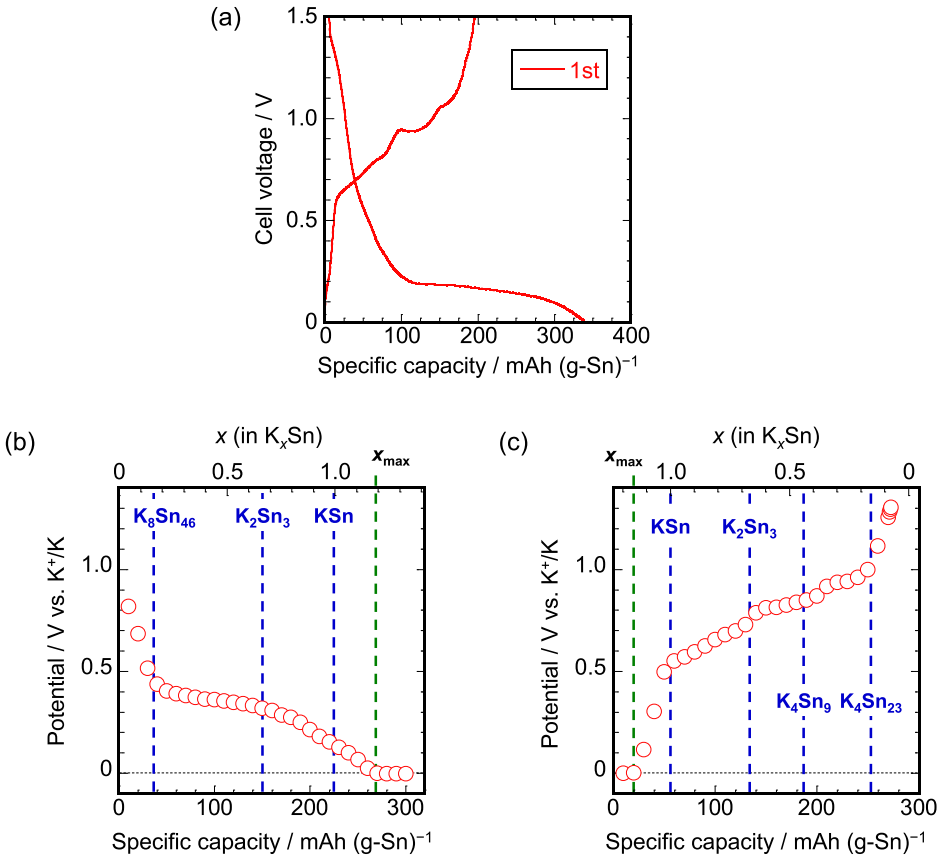

Fig. S1 (a) Initial charge–discharge curves of the Sn/AB/PAI electrode in K[FSA]–[C_3C_1pyrr][FSA] ionic liquid electrolyte at 298 K. Charge–discharge rate: 20 mA (g-Sn)$^{-1}$. Subsequent GITT plots for (b) charging and (c) discharging processes in the 2nd cycle.

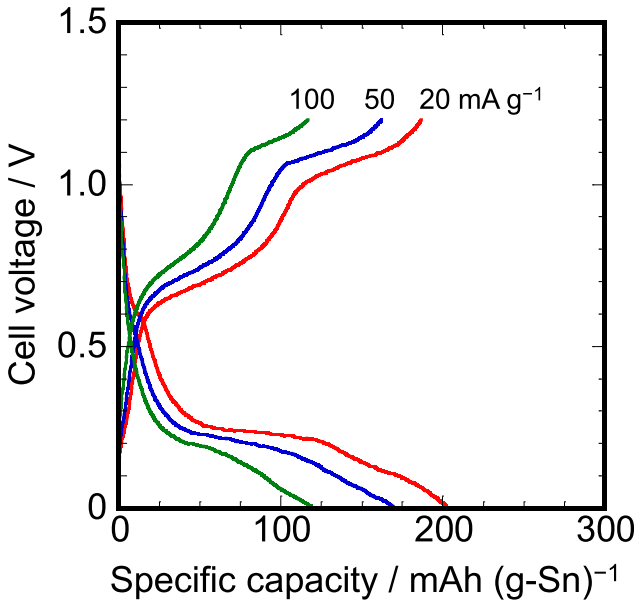

Fig. S2 Rate capability of the Sn/AB/PAI electrode in K[FSA]–[C_3C_1pyrr][FSA] ionic liquid electrolyte at 298 K. Charge–discharge rates: 20, 50, and 100 mA $(g\text{-}Sn)^{-1}$.

The Sn/AB/PAI electrode exhibited the discharge capacities of 187, 162, and 117 mAh $(g\text{-}Sn)^{-1}$ at charge–discharge rates of 20, 50, and 100 mA $(g\text{-}Sn)^{-1}$, respectively.

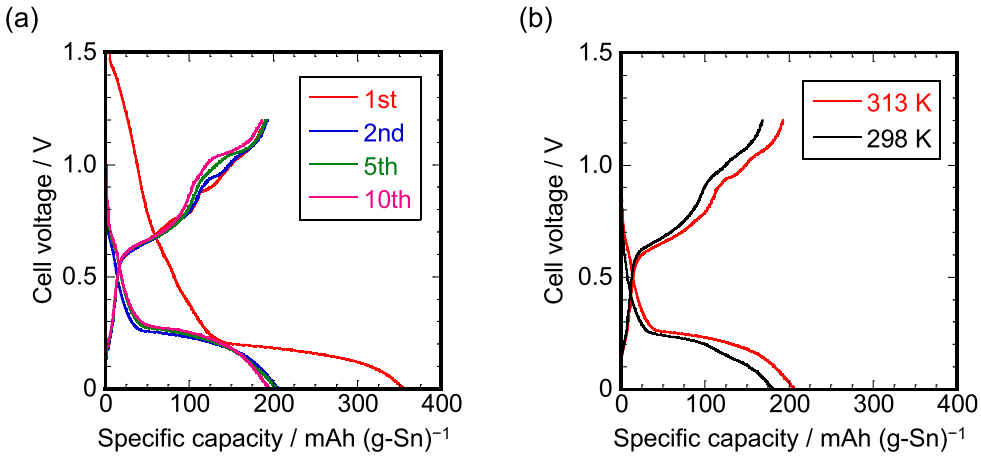

Fig. S3 (a) Charge–discharge curves of the Sn/AB/PAI electrode in K[FSA]–[C_3C_1pyrr][FSA] ionic liquid electrolyte for 10 cycles at 313 K. (b) A comparison of charge–discharge curves in the 2nd cycle at 298 K and 313 K. Charge–discharge rate: 20 mA (g-Sn)$^{-1}$.

References

[a] T. B. Massalski, *Binary Alloy Phase Diagrams, second ed.*, ASM International, Ohio, 1990.; J. Sangster and C.W. Bale, *J. Phase. Equilib.*, 1998, **19**, 67–69.

[b] J. Gallmeier, H. Schaefer, A. Weiss, *Z. Naturf. B*, 1969, **24**, 665–667.

[c] T. F. Faessler, C. Z. Kronseder, *Anorg. Allg. Chem.*, 1998, **624**, 561–568.

[d] C. Hoch, M. Wendorff and C. Röhr, *Acta Cryst.*, 2002, **C58**, i45–i46.

[e] I. F. Hewaidy, E. Busmann and W. Z. Klemm, *Anorg. Allg. Chem.*, 1964, **328**, 283–293.